Cathelicidin LL-37 Activates Human Keratinocyte Autophagy through the $P2X_7$, Mechanistic Target of Rapamycin, and MAPK Pathways

Risa Ikutama[1,2,5], Ge Peng[1,2,5], Saya Tsukamoto[1,2], Yoshie Umehara[1], Juan Valentin Trujillo-Paez[1], Hainan Yue[1,2], Hai Le Thanh Nguyen[1,2], Miho Takahashi[1,2], Shun Kageyama[3], Masaaki Komatsu[3], Ko Okumura[1], Hideoki Ogawa[1], Shigaku Ikeda[1,2] and François Niyonsaba[1,4]

Human cathelicidin LL-37 is a multifunctional antimicrobial peptide that exhibits antimicrobial and immunomodulatory activities. LL-37 regulates skin barrier function and was recently reported to activate autophagy in macrophages. Because autophagy deficiency is associated with skin diseases characterized by a dysfunctional epidermal barrier, we hypothesized that LL-37 might regulate the skin barrier through autophagy modulation. We showed that LL-37 activated autophagy in human keratinocytes and three-dimensional skin equivalent models as indicated by increases in LC3 puncta formation, decreases in p62, and autophagosome and autolysosome formation. LL-37–induced autophagy was suppressed by $P2X_7$ receptor, adenosine monophosphate–activated protein kinase, and unc-51-like kinase 1 inhibitors, suggesting that the $P2X_7$, adenosine monophosphate–activated protein kinase, and unc-51-like kinase 1 pathways are involved. Moreover, LL-37 enhanced the phosphorylation of adenosine monophosphate–activated protein kinase and unc-51-like kinase 1. In addition, LL-37–mediated autophagy involves the mechanistic target of rapamycin and MAPK pathways. Interestingly, the LL-37–induced distribution of tight junction proteins and improvement in the tight junction barrier were inhibited in autophagy-deficient keratinocytes and keratinocytes and skin models treated with autophagy inhibitors, indicating that the LL-37–mediated tight junction barrier is associated with autophagy activation. Collectively, these findings suggest that LL-37 is a potential therapeutic target for skin diseases characterized by dysfunctional autophagy and skin barriers.

Journal of Investigative Dermatology (2023) **143,** 751–761; doi:10.1016/j.jid.2022.10.020

INTRODUCTION

Antimicrobial peptides are small proteins with pleiotropic functions. Among antimicrobial peptides, cathelicidins and human β-defensins are key players in the cutaneous immune system (Niyonsaba et al., 2017). Human cationic antibacterial protein is a unique cathelicidin found in humans, and its proteolytic cleavage by proteinase-3 in neutrophils and kallikreins 5 and 7 in keratinocytes (KCs) leads to the release of LL-37 (Kuroda et al., 2015).

[1]*Atopy (Allergy) Research Center, Juntendo University Graduate School of Medicine, Tokyo, Japan;* [2]*Department of Dermatology and Allergology, Juntendo University Graduate School of Medicine, Tokyo, Japan;* [3]*Department of Physiology, Juntendo University Graduate School of Medicine, Tokyo, Japan; and* [4]*Faculty of International Liberal Arts, Juntendo University, Tokyo, Japan*

[5]*These authors contributed equally to this work.*

Correspondence: François Niyonsaba, Atopy (Allergy) Research Center, Juntendo University Graduate School of Medicine, 2-1-1 Hongo, Bunkyo-ku, Tokyo 113-8421, Japan. E-mail: francois@juntendo.ac.jp

Abbreviations: AD, atopic dermatitis; AMPK, adenosine monophosphate–activated protein kinase; Ca^{2+}, calcium ion; KC, keratinocyte; mTOR, mechanistic target of rapamycin; TER, transepithelial electrical resistance; TJ, tight junction; ULK1, unc-51-like kinase 1

Received 6 May 2022; revised 30 September 2022; accepted 18 October 2022; accepted manuscript published online 28 November 2022; corrected proof published online 20 December 2022

LL-37 is expressed in various cells, including KCs, either constitutively or by induction after infection, injury, and inflammation (Kuroda et al., 2015). In addition to its antimicrobial activity, LL-37 exerts a wide range of immunomodulatory functions, including the regulation of cell proliferation and differentiation and modulation of the skin barrier (Chieosilapatham et al., 2018). Furthermore, LL-37 is involved in the pathogenesis of skin diseases such as psoriasis and atopic dermatitis (AD) (Niyonsaba et al., 2017). In addition, LL-37 activates autophagy in macrophages (Rekha et al., 2015).

Autophagy is a cellular process that removes dysfunctional proteins and delivers them to lysosomes for degradation and recycling (Ohsumi, 2001). The morphological characteristic of autophagy is the presence of autophagosomes/autolysosomes. On a molecular level, the mechanistic target of rapamycin (mTOR) is one of the most important regulators of autophagy (Wang and Zhang, 2019). mTOR actively suppresses autophagy, whereas its inactivation initiates autophagy. mTOR is associated with the phosphorylation of antimicrobial peptide–activated protein kinase (AMPK) (Kim et al., 2011; Schmeisser and Parker, 2019). After autophagy initiation, AMPK is activated and promotes autophagy through the activation of unc-51-like kinase 1 (ULK1), eventually leading to autophagy induction (Kim et al., 2011).

Moreover, autophagosome formation involves the post-transcriptional modification of LC3, which consists of LC3-I and LC3-II, located both outside and inside autophagosomes (Yoshii and Mizushima, 2017). Because the amount of LC3-II reflects the number of autophagosomes, LC3-II is the best-known marker for monitoring the formation of autophagosomes (Kabeya et al., 2000). Furthermore, sequestosome 1/p62 recognizes and shuttles ubiquitinated protein cargo for degradation and interacts with LC3-II (Rogov et al., 2014). Because p62 is constantly degraded during autophagy activation, p62 reduction is an indicator of autophagy activation (Klionsky et al., 2021).

The skin lesions of psoriasis and AD display reduced LC3, accumulated p62, and lysosomal dysfunction (Akinduro et al., 2016; Klapan et al., 2021; Peng et al., 2022; Sukseree et al., 2021), suggesting that autophagy deficiency is associated with skin diseases characterized by defects in the epidermal barrier and differentiation. Because LL-37 improves the epidermal barrier and differentiation (Aberg et al., 2008; Akiyama et al., 2014) and 1,25-dihydroxyvitamin D3, an inducer of LL-37, activates autophagy (Yuk et al., 2009), we hypothesized that LL-37 might contribute to the modulation of KC autophagy.

In addition, LL-37 markedly activated autophagy in human KCs and three-dimensional skin equivalent models. The LL-37–induced improvement in the tight junction (TJ) barrier was abolished by autophagy inhibition, suggesting that LL-37–mediated regulation of the TJ barrier is associated with autophagy activation. Because LL-37 strengthens the epidermal barrier and modulates KC differentiation, LL-37–mediated autophagy activation suggests the potential use of LL-37 as a therapeutic target for the treatment of diseases with compromised epidermal barrier and autophagy.

RESULTS

LL-37 activates autophagy in human KCs

To evaluate the effect of LL-37 on autophagy, we monitored the number of LC3-positive vesicles in KCs stimulated with LL-37. Immunostaining revealed that after the treatment of KCs with LL-37, the number of LC3 puncta was significantly increased compared with that of nonstimulated cells (Figure 1a), suggesting that LL-37 induces autophagy. Immunoblotting was used to investigate the LC3-I–LC3-II conversion and showed that the LL-37–treated KCs displayed increases in the LC3-II/LC3-I ratios. To exclude the possibility that LL-37 blocks lysosomal degradation rather than inducing autophagic flux, the LC3-II levels were assessed in the presence or absence of the lysosomal inhibitors E64d and pepstatin A. The treatment with E64d and pepstatin A increased the accumulation of LC3-II in the LL-37–stimulated cells, suggesting that LL-37 promoted autophagic flux (Figure 1b). In addition, LL-37 decreased the p62/GAPDH ratio (Figure 1c). Furthermore, the ultrastructural analysis of electron microscopy showed that after the treatment of KCs with LL-37, multiple autophagosome-like vacuoles were observed, revealing the presence of autophagosomes (yellow arrowheads) and autolysosomes (green arrowheads) (Figure 1d). Furthermore, confocal images confirmed that LL-37 increased the number of LC3 puncta, and p62 puncta colocalized with LC3-positive structures, suggesting that p62-positive cargo was recruited within autophagosomes (Figure 1e). We also examined whether LL-37 induced autophagosome–lysosome fusion by assessing the colocalization of LC3 puncta with LAMP-1. There were increases in the colocalization of LC3 puncta and LAMP-1 (Figure 1f), indicating that the numbers of autolysosomes increased after the LL-37 stimulation.

Because the LL-37 levels are estimated to be 4.5 μg/ml in normal skin (Murakami et al., 2002) and 1.38 mg/ml in psoriatic skin lesions (Ong et al., 2002), we assume that the LL-37 concentrations used in this study are physiologically relevant.

LL-37 activates autophagy in KCs through the $P2X_7$ receptor

LL-37 involves various receptors, including the purinergic receptor $P2X_7$, which induces autophagy through the mTOR pathway (Fabbrizio et al., 2017). The pretreatment of KCs with KN-62, a selective antagonist of $P2X_7$ (Bian et al., 2013), resulted in a reduction in LL-37–induced increases in LC3 puncta (Supplementary Figure S1a). The inhibitory effect of KN-62 on autophagy was confirmed by immunoblotting because the LC3-II/LC3-I ratios were suppressed to the baseline levels (Figure 2a), indicating that LL-37 activates autophagy in KCs through the $P2X_7$ receptor.

LL-37 regulates autophagy through the mTOR and AMPK/ULK1 pathways

As shown in the upper panels of Figure 2b, we confirmed that rapamycin, a potent and selective inhibitor of mTOR, increased the LC3-II/LC3-I ratios in KCs similar to LL-37. The incubation of KCs with LL-37 resulted in the inhibition of mTOR phosphorylation, similar to the effects of rapamycin (middle panels). Furthermore, LL-37 suppressed the phosphorylation of S6K, the major mTOR downstream substrate at Thr389 and Thr421 (lower panels). Interestingly, the LL-37–induced inhibition of mTOR and S6K was restored to the baseline levels by pretreatment of KCs with KN-62 (Figure 2c), suggesting a link between the $P2X_7$ and mTOR pathways.

Supplementary Figure S1b shows that the stimulation with LL-37 markedly enhanced the phosphorylation of AMPK, with a peak at 30 minutes (left panel), and of ULK1 from 5 to 60 minutes (right panel). We investigated whether LL-37–induced autophagy depended on these pathways by pretreating cells with Compound C (AMPK inhibitor) and SBI-0206965 (ULK1 inhibitor). Both inhibitors significantly suppressed LL-37–induced LC3-II and increased the p62 levels (Figure 2d). AMPK and ULK1 likely function downstream of $P2X_7$ because the treatment of KCs with KN-62 reduced LL-37–induced phosphorylation of AMPK and ULK1 (Figure 2e). In addition, the finding that Compound C suppressed ULK1 phosphorylation and increased mTOR phosphorylation further confirms that AMPK functions upstream of the ULK1 and mTOR pathways (Figure 2f). These data indicate that the AMPK and ULK1 pathways are important for LL-37–mediated KC autophagy.

LL-37 regulates autophagy through MAPK pathways

We confirmed that LL-37 induced MAPK activation as follows: extracellular signal–regulated kinase and c-Jun NH_2-terminal kinase at 5 minutes and p38 at 60 minutes after stimulation (Supplementary Figure S1c). To examine whether

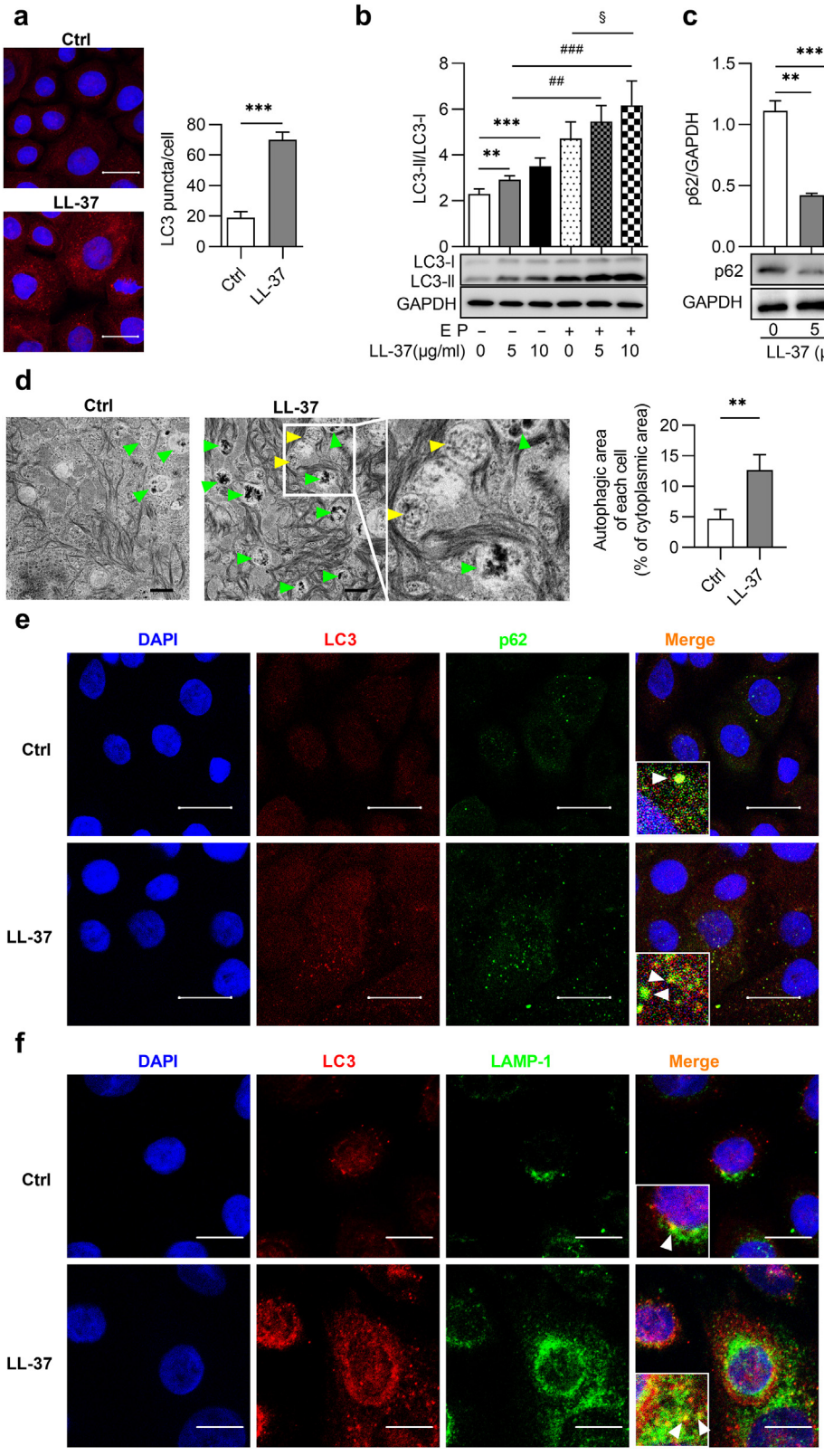

Figure 1. LL-37 activates keratinocyte autophagy. (**a**) Keratinocytes were stimulated with 10 μg/ml LL-37 for 12 hours. LC3 puncta were visualized by immunofluorescence. (**b, c**) Keratinocytes were stimulated with LL-37 in the absence or presence of 10 μg/ml EP for 12 hours. The expression of (**b**) LC3-I, LC3-II, and (**c**) p62 was determined by immunoblotting. (**d**) Representative electron microscopy images of keratinocytes stimulated with 10 μg/ml LL-37 for 12 hours. (**e, f**) Colocalization of LC3 with p62 or LAMP-1 was visualized by immunofluorescence. The white arrows show the colocalization area. $^{**}P < 0.01$ and $^{***}P < 0.001$ versus the nonstimulated group, $^{\#\#}P < 0.01$ and $^{\#\#\#}P < 0.001$ versus the group without EP, and $^{\S}P < 0.05$ versus the EP-treated nonstimulated group. n = 3. Ctrl, control; EP, E64d and pepstatin A.

MAPK activation is indeed required for LL-37–induced KC autophagy, cells were pretreated with U0126 (extracellular signal–regulated kinase inhibitor), c-Jun NH_2-terminal kinase inhibitor II, and SB203850 (p38 inhibitor). As shown in Supplementary Figure S1d, all MAPK inhibitors significantly attenuated the number of LC3 puncta in the LL-37–stimulated KCs. Similarly, immunoblotting confirmed that these inhibitors reduced the LC3-II/LC3-I ratios (Figure 2g).

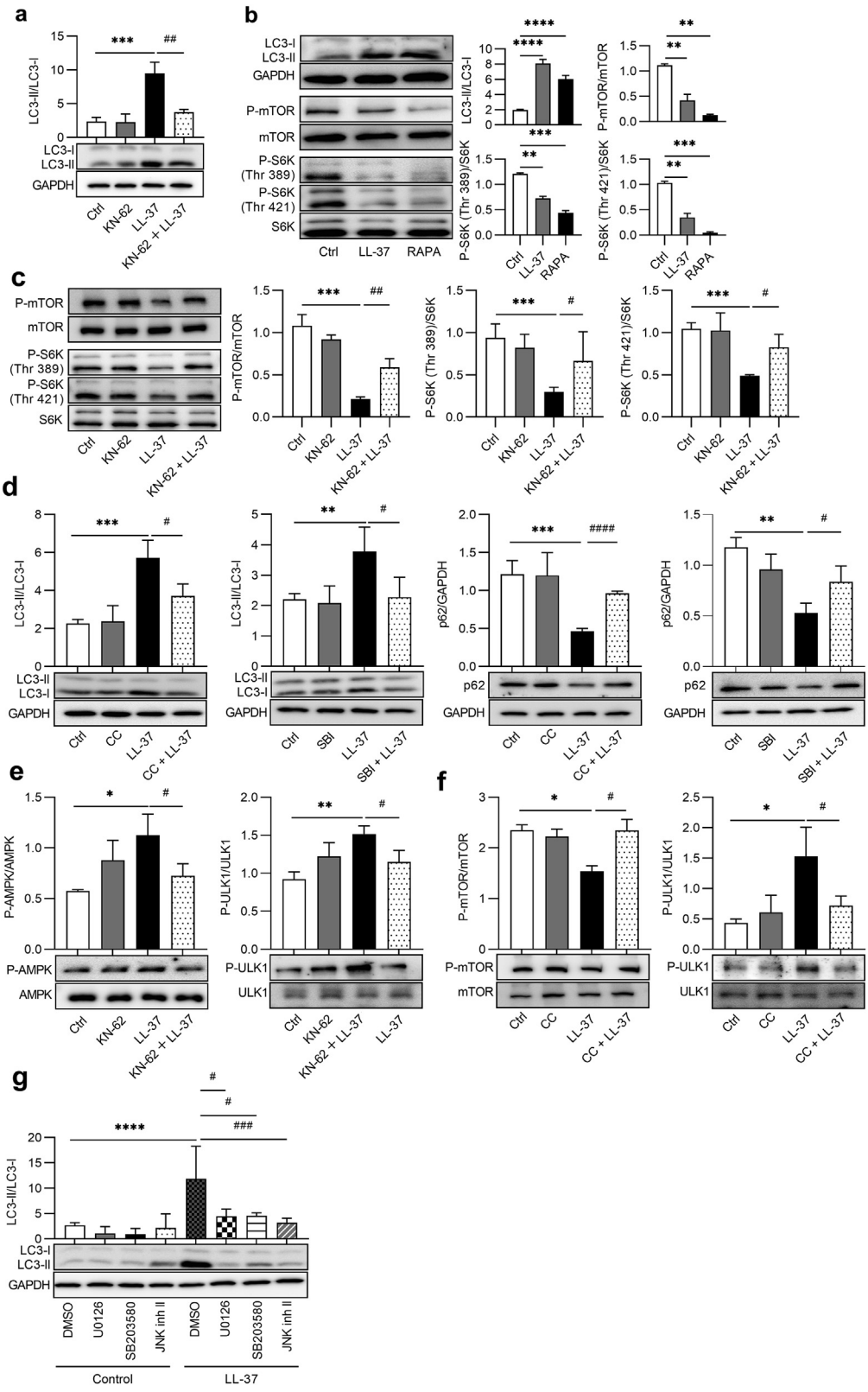

Figure 2. LL-37 induces autophagy through the P2X$_7$/mTOR and AMPK/ULK1/MAPK pathways. (**a**) Keratinocytes pretreated with 50 nM KN-62 for 1 hour were incubated with 10 μg/ml LL-37 for 12 hours. LC3-I and LC3-II expression was determined by immunoblotting. (**b**) Keratinocytes were stimulated with 10 μg/ml LL-37 or 0.2 μM RAPA for 12 hours. The expression of LC3-I, LC3-II, and P-mTOR and S6K was determined by immunoblotting. (**c**) Keratinocytes pretreated with KN-62 were incubated with 10 μg/ml LL-37 for 12 hours. P-mTOR and S6K were determined by immunoblotting. (**d**) Keratinocytes were pretreated with 100 nM CC or 100 nM SBI for 1 hour and incubated with 10 μg/ml LL-37 for 12 hours. LC3-I, LC3-II, and p62 expressions were determined by immunoblotting. (**e, f**) Keratinocytes were pretreated with 50 nM KN-62 or CC for 1 hour and stimulated with 10 μg/ml LL-37 for 30 minutes. (**e**) P-AMPK and ULK1 and (**f**) P-ULK1 were determined by immunoblotting. (**g**) Keratinocytes were pretreated with U0126, SB203580, c-Jun NH_2-terminal kinase inhibitor II (2 μM each) or 0.01% DMSO for 2 hours, followed by incubation with 10 μg/ml LL-37 for 12 hours. The expressions of LC3-I and LC3-II was determined by immunoblotting. $^{*}P < 0.05$, $^{**}P < 0.01$, $^{***}P < 0.001$, and $^{****}P < 0.0001$ versus the nonstimulated groups and $^{\#}P < 0.05$, $^{\#\#}P < 0.01$, $^{\#\#\#}P < 0.001$, and $^{\#\#\#\#}P < 0.0001$ versus the group without inhibitors. n = 3–6. AMPK, adenosine monophosphate–activated protein kinase; CC, Compound C; JNK inh II, c-Jun NH_2-terminal kinase inhibitor II; mTOR, mechanistic target of rapamycin; P-AMPK, phosphorylated adenosine monophosphate–activated protein kinase; P-mTOR, phosphorylated mechanistic target of rapamycin; P-S6K, phosphorylated S6K; P-ULK1, phosphorylated unc-51-like kinase 1; RAPA, rapamycin; SBI, SBI-0206965; ULK1, unc-51-like kinase 1.

LL-37 improves the TJ barrier in KCs through the activation of autophagy

Autophagy-activating peptide was recently shown to reduce transepidermal water loss, suggesting that autophagy plays a role in the maintenance of the skin barrier (Lee et al., 2021). However, the association between autophagy and the TJ barrier remains unclear. Because an elevation in the extracellular calcium ion (Ca^{2+}) concentration in KCs leads to TJ

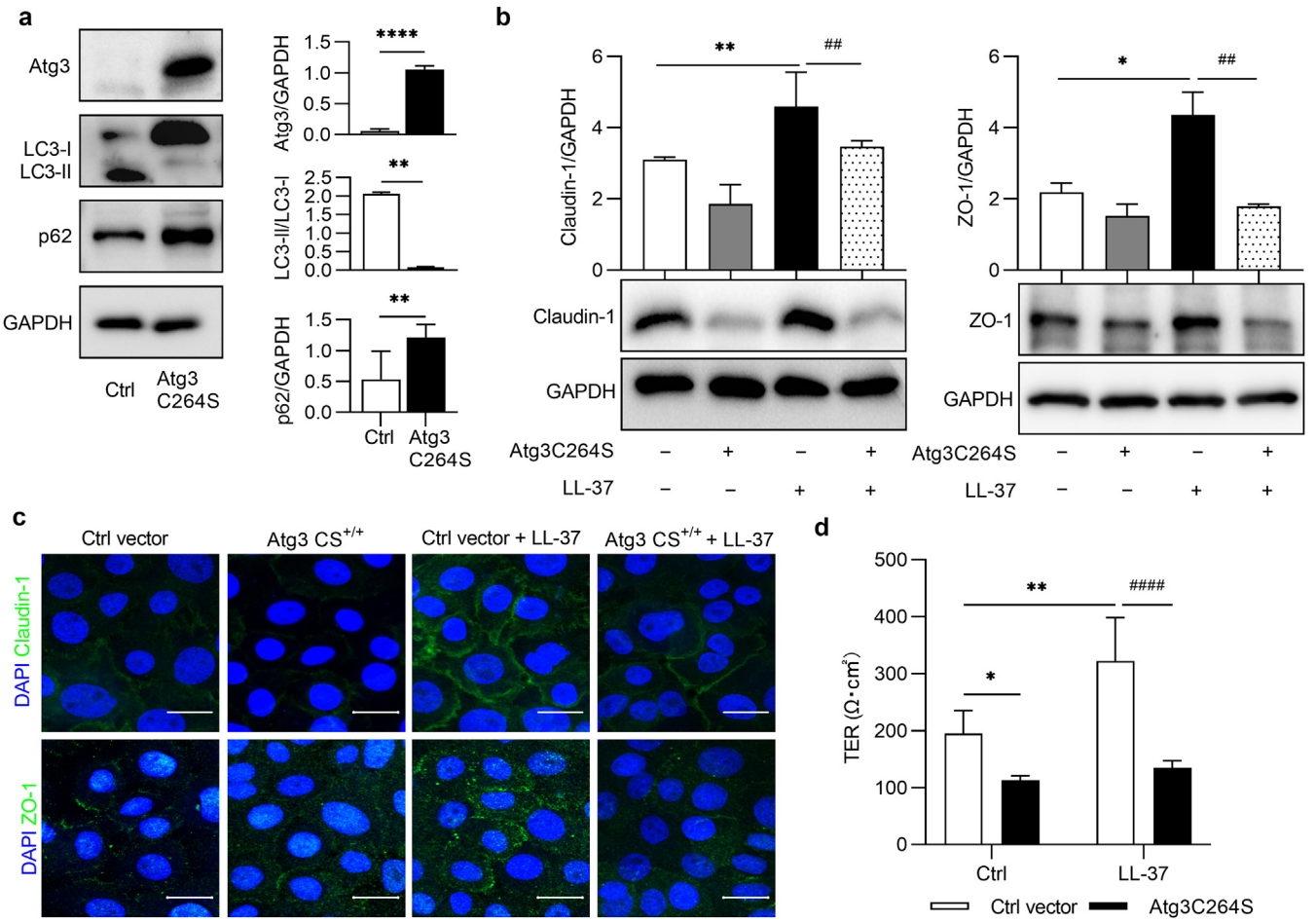

Figure 3. LL-37–mediated tight junction induction is associated with autophagy activation. (**a**) Keratinocytes were infected with an *Atg3C264S*-mutant adenovirus for 24 hours. The expression of Atg3, LC3-I, LC3-II, and p62 was determined by immunoblotting. Infected cells were stimulated with LL-37 for 12 hours, and the expression of claudin-1 and ZO-1 was determined by (**b**) immunoblotting, whereas their intracellular distribution was visualized by (**c**) immunofluorescence. (**d**) Keratinocytes grown on Transwell filters were infected with Atg3 C264S and then stimulated with 10 μg/ml LL-37. TER was measured at 96 hours after stimulation. $^{*}P < 0.05$, $^{**}P < 0.01$, and $^{***}P < 0.001$ versus the noninfected or stimulated groups and $^{\#\#\#}P < 0.001$ and $^{\#\#\#\#}P < 0.0001$ versus the groups without Atg3C264S. n = 3. Ctrl, control; TER, transepithelial electrical resistance.

formation and improvement in the permeability barrier (Yuki et al., 2007), we cultured KCs in high (1.8 mM) Ca^{2+} concentrations to mimic the second layer of stratum granulosum cells, where functional TJs are formed (Yoshida et al., 2013). Approximately 32 and 30% of the KCs still expressed the basal layer markers keratin 5 and keratin 14, respectively, whereas approximately 23% expressed the proliferation marker Ki-67, and the treatment of KCs with LL-37 did not affect these markers (Supplementary Figure S2a–c). In contrast, the LL-37–treated KCs showed a twofold increase in the differentiation-specific marker keratin 1 (Supplementary Figure S2d). During Ca^{2+}-induced KC differentiation, LL-37 further increased LC3-II/LC3-I ratios (Supplementary Figure S3). To test whether autophagy disruption causes TJ barrier dysfunction, we used an adenovirus system to infect KCs with Atg3C264S mutation, which blocks autophagy activation (Sou et al., 2008). We confirmed that Atg3C264S was sufficiently expressed in KCs (Figure 3a). Atg3 inhibition prevented the conversion of LC3-I to LC3-II and increased the levels of p62 in KCs (Figure 3a), indicating autophagy deficiency. Interestingly, as shown in Figure 3b, the LL-37–mediated upregulation of claudin-1 (left panel) and ZO-1 (right panel) was noticeably reduced in the KCs infected with Atg3C264S. The LL-37–induced intracellular distribution of claudin-1 and ZO-1 was also abolished in the Atg3C264S-infected KCs, suggesting an impaired TJ barrier in these cells (Figure 3c). This finding was confirmed by the observation that LL-37–stimulated Atg3C264S-infected KCs exhibited lower values of transepithelial electrical resistance (TER) (Figure 3d), indicating that autophagy activation is required for the LL-37–mediated regulation of TJ barrier function.

Furthermore, autophagy inhibitors, such as E64d and pepstatin A, chloroquine, and wortmannin, suppressed the LL-37–induced upregulation of claudin-1 and ZO-1 (Figure 4a) and reduced the intracellular distribution of claudin-1 and ZO-1 (Figure 4b) and TER (Figure 4c). These inhibitors also suppressed other TJ proteins, such as claudin-4 and occludin (Supplementary Figure S4). Importantly, KN-62 noticeably reduced LL-37–induced claudin-1 and ZO-1 expression and the TER values (Supplementary Figure S5a and b).

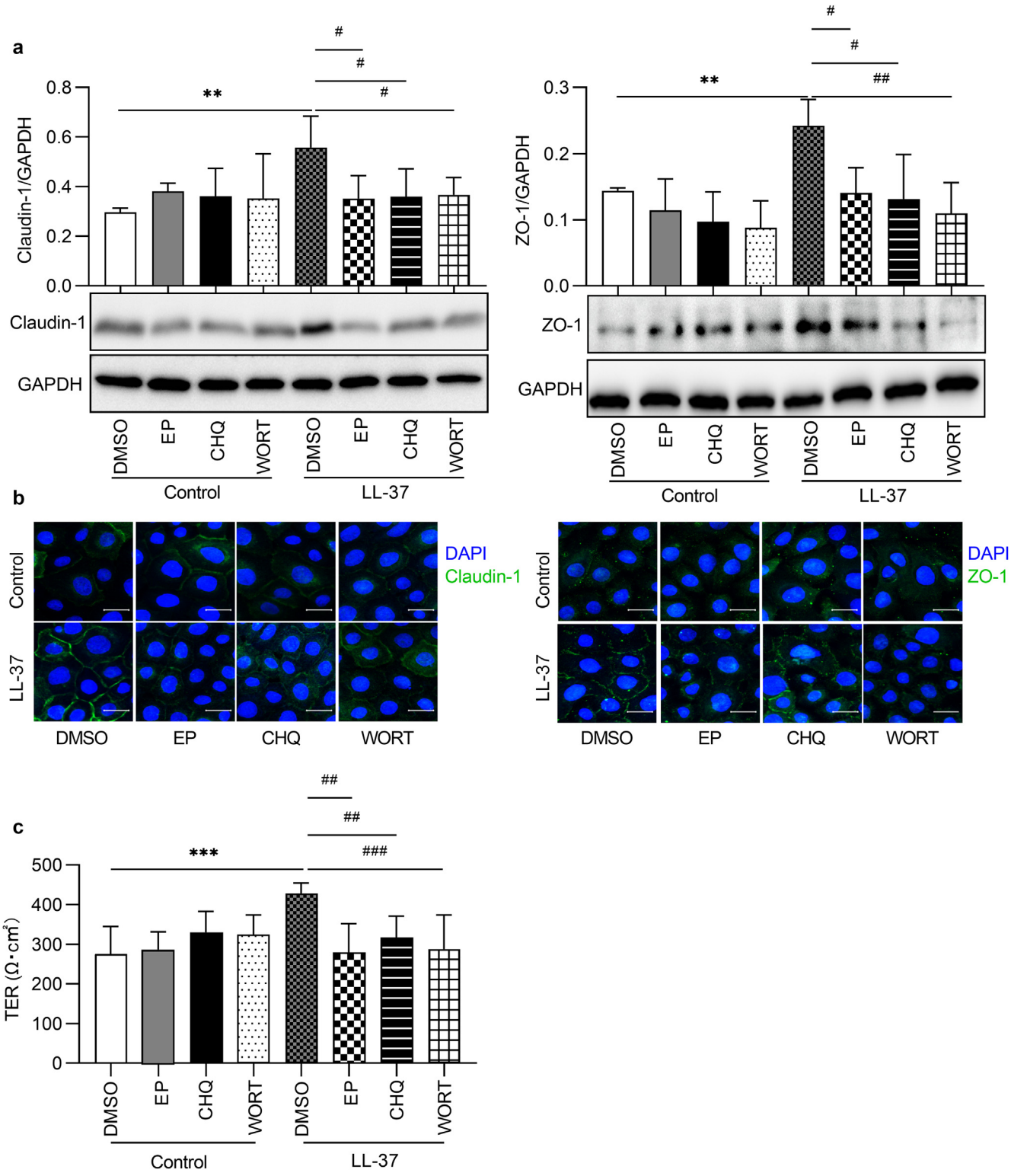

Figure 4. LL-37 regulates tight junctions through autophagy activation. Keratinocytes were treated with 10 μg/ml EP, 200 nM CHQ, and 200 nM WORT or 0.1% DMSO for 2 hours and then stimulated with 10 μg/ml LL-37 for 12 hours. (**a**) The expression of claudin-1 and ZO-1 was determined by immunoblotting. (**b**) The intracellular distribution of claudin-1 and ZO-1 was visualized by immunofluorescence. (**c**) TER values were measured in keratinocytes pretreated with various inhibitors and stimulated with LL-37. The data represent the TER at 96 hours. $^{**}P < 0.01$ versus the nonstimulated group, $^{***}P < 0.001$ versus the nonstimulated groups, and $^{\#}P < 0.05$, $^{\#\#}P < 0.01$, and $^{\#\#\#}P < 0.001$ versus the groups without inhibitors. n = 4–5. CHQ, chloroquine; EP, E64d and pepstatin A; TER, transepithelial electrical resistance; WORT, wortmannin.

Subsequently, we examined whether LL-37 induces KC differentiation, adherens junction, or desmosome-related proteins through the autophagy pathway. LL-37–induced terminal differentiation markers, including FLG, involucrin, keratin 1, keratin 10, and transglutaminase 1, were abolished by the autophagy inhibitors (Supplementary Figure S6).

However, LL-37 failed to increase the expression of adherens junction β-catenin and E-cadherin or desmosome-related proteins, such as desmoglein 1, desmocollin 1, and desmoplakin 1/2, excluding the involvement of LL-37 in the regulation of adherens junctions or desmosome-related proteins.

LL-37 induces autophagy and regulates the TJ barrier through autophagy activation in human skin equivalent models

To confirm the relevance of our data under physiological conditions, LL-37–mediated regulation of TJs through autophagy activation was further evaluated using human skin equivalents. Tissues grown at the air-lifted interface display a fully differentiated and stratified epithelium after 7 days of culture (Koria and Andreadis, 2006). Treatment of the skin equivalents with autophagy inhibitors for 3 days during epidermal differentiation and stratification phase (days 2–5) resulted in a thinner epithelium. The stimulation of skin equivalents with LL-37 did not change the thickness of epithelium (Supplementary Figure S7a), indicating that epidermal differentiation and stratification were inhibited after autophagy inactivation. Skin equivalents treated with LL-37 for 3 days (days 4–7) in the absence of autophagy inhibitors displayed thicker epithelium than the control skin; however, the addition of autophagy inhibitors did not affect the epithelium thickness (Supplementary Figure S7b). The quality of the skin equivalents was confirmed by the staining of a nuclear proliferation marker Ki-67 (Supplementary Figure S7c) and a differentiated marker keratin 1 (Supplementary Figure S7d). All skin equivalents showed nuclear Ki-67 in the basal layer and keratin 1 from suprabasal to cornified layers, suggesting a complete differentiation and stratification of the skin tissues (Supplementary Figure S7c and d). Consistent with the result shown in Supplementary Figure S7c and d and Supplementary Figure S7, LL-37 did not affect Ki-67 expression; however, it upregulated keratin 1 levels (Supplementary Figure S7c and d), indicating that the increased thickness of skin equivalents by LL-37 (Supplementary Figure S7b) may be due to an increased epidermal differentiation rather than hyperproliferation. To further investigate the effect of LL-37 on TJs and autophagy, we treated skin equivalents for 3 days (days 4–7). The treatment of skin equivalents with LL-37 increased LC3, decreased p62, and induced the colocalization of LC3 and p62 (Figure 5a), suggesting autophagy activation. Moreover, LL-37–induced claudin-1 and ZO-1 expression was suppressed by autophagy-specific inhibitors (Figure 5b). To evaluate the potential role of LL-37 in the regulation of TJ barrier function, skin equivalents were cultured with an NHS-LC-biotin paracellular tracer from the dermal side as previously described (Yuki et al., 2007), followed by immunofluorescence staining of claudin-1 (green). In the LL-37–treated sections, the diffusion of the tracer (red) from the basal to the upper layer was blocked (arrowheads) by the intact TJ barrier, represented by colocalization of claudin-1 and biotin tracer. As expected, in the presence of autophagy inhibitors, the tracer diffused and passed through the outermost layer of the skin equivalents as shown by a reduced number of biotin stops (Figure 5c), confirming the in vitro findings that LL-37 may improve KC TJ barrier function through the activation of autophagy.

DISCUSSION

In KCs, autophagy is required for epidermal terminal differentiation and homeostasis (Klionsky and Emr, 2000). Autophagy dysfunction has been associated with the pathogenesis of skin disorders, such as psoriasis and AD, whose pathological mechanisms are associated with LL-37. In psoriasis, the negative marker of autophagy p62 is upregulated (Lee et al., 2011), various *ATG16L1* SNPs are associated with the disease (Douroudis et al., 2012), the inhibition of autophagy exacerbates psoriasis (Kim and Del Rosso, 2010), and the induction of autophagy improves psoriasis (Kim et al., 2021). In addition, p62 accumulates in AD, and p62 inactivation is associated with a reduction in epidermal thickening, differentiation defects, and immune cell infiltration in AD skin lesions (Sukseree et al., 2021). Because LL-37 participates in modulatory functions in KCs, we hypothesized that LL-37 might regulate KC autophagy. In this study, LL-37 activated KC autophagy, which involves the $P2X_7$ receptor, activation of the AMPK/ULK1 pathway, inhibition of the mTOR pathway, and activation of MAPK pathways. Interestingly, the LL-37–mediated improvement in the TJ barrier was associated with autophagy activation.

Several signaling pathways regulate autophagy, including mTOR, AMPK, and ULK1. Although mTOR is a negative modulator of autophagy, AMPK positively regulates autophagy by activating ULK1 and inhibiting the mTOR complex (Zhao et al., 2016). We found that LL-37 inhibited mTOR phosphorylation and induced AMPK and ULK1 phosphorylation. AMPK is a crucial regulator of KC autophagy on LL-37 stimulation because an AMPK inhibitor reduced the phosphorylation of ULK1, suggesting that ULK1 is a downstream signal of AMPK. ULK1 initiates the autophagic process, and the activation of the AMPK/ULK1 pathway is a key regulator of autophagy in several pathological conditions, including infections (Fan et al., 2015).

In addition, MAPK pathways are important in autophagy regulation. A recent report showed that in an in vitro psoriasiform KC model, the MAPK pathways were activated, and the knockdown of these pathways suppressed autophagic flux in KCs (Wang et al., 2021). This observation is consistent with those of previous studies showing that MAPK pathways were required for autophagy activation in macrophages (Hara et al., 2006; Harris, 2011). The inhibition of extracellular signal–regulated kinase attenuates LC3 puncta in HepG2 cells (Tong et al., 2015), and c-Jun NH_2-terminal kinase activation is necessary for autophagy activation in nasopharyngeal carcinoma cells and squamous cell carcinoma cells (Li and Johnson, 2012; Sun et al., 2011). In contrast, p38 plays opposing roles in the regulation of autophagy because the activation of the p38 pathway leads to autophagy stimulation in HeLa cells (Zhou et al., 2012), whereas its inhibition promotes autophagy in TNF-α–treated L929 cells (Ye et al., 2011).

LL-37 induces autophagy in macrophages (Yuk et al., 2009). The most relevant LL-37–mediated effects are mainly controlled through various cell surface receptors, including the $P2X_7$ receptor (Elssner et al., 2004), which

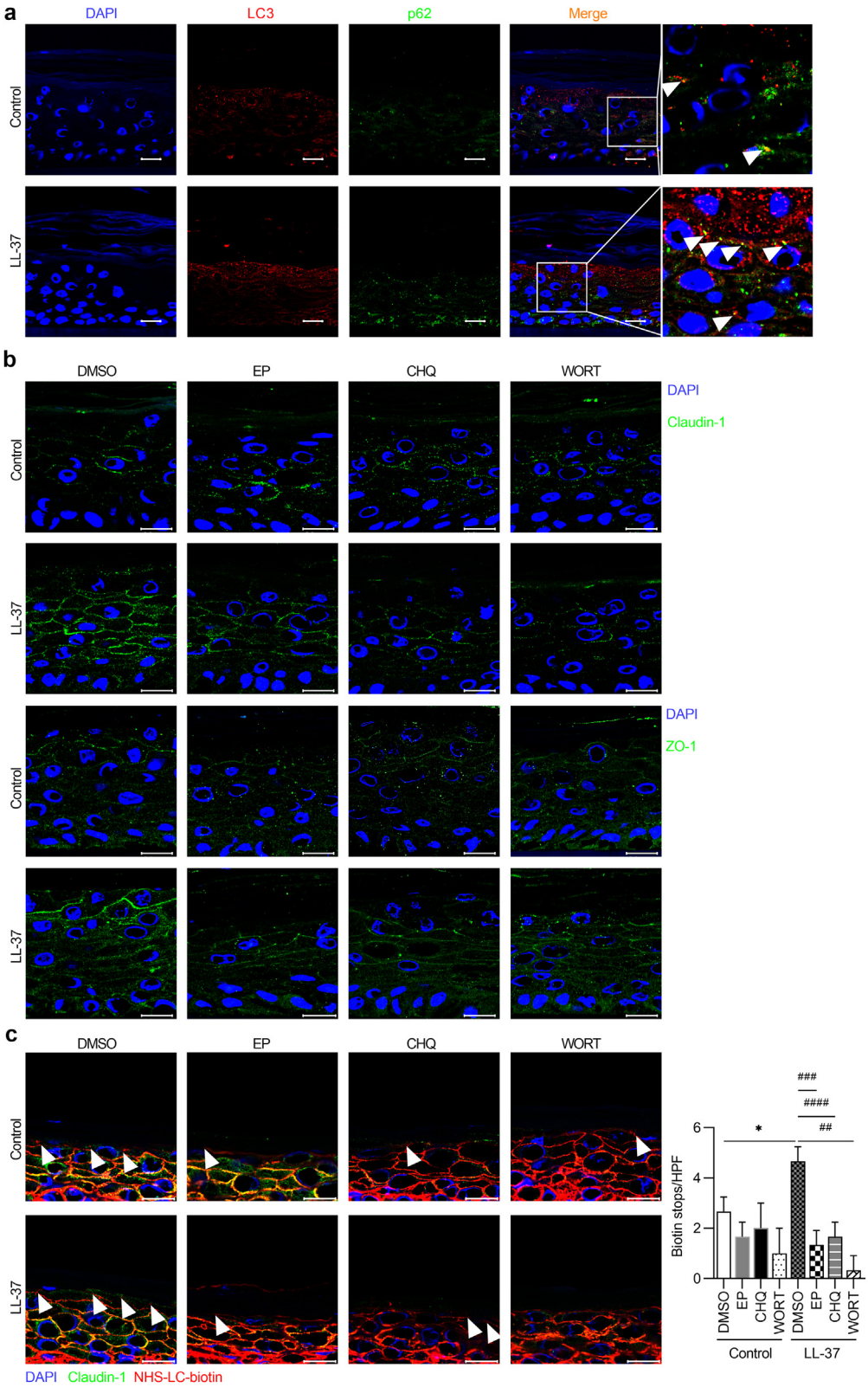

Figure 5. LL-37 induces autophagy and regulates the TJ barrier through autophagy activation in human skin equivalents. (**a**) Skin models were stimulated with 10 μg/ml LL-37 for 72 hours, and LC3 and p62 were visualized by immunofluorescence. (**b**) Skin models were pretreated with 10 μg/ml EP, 200 nM CHQ, and 200 nM WORT or 0.1% DMSO with or without 10 μg/ml LL-37 for 72 hours. The intracellular distribution of claudin-1 and ZO-1 was visualized by immunofluorescence. (**c**) Representative immunofluorescence images of the colocalization of claudin-1 (left) and biotin tracer and quantification of the biotin tracer stops (right) per HPF in skin equivalents. The biotin tracer stops are indicated by white arrowheads. Bar = 20 μm. CHQ, chloroquine; EP, E64d and pepstatin A; HPF, high power field; TJ, tight junction; WORT, wortmannin.

regulates autophagy in various cell types, including epithelial cells (Fabbrizio et al., 2017). In fact, $P2X_7$ is a positive regulator of autophagy in monocytes and macrophages (Young et al., 2015), whereas its activation mediates mTOR phosphorylation in microglial cells, resulting in decreases in lysosomal functions (Fabbrizio et al., 2017). In this study, a $P2X_7$-specific antagonist suppressed LC3 puncta, increased the mTOR pathway, and inhibited AMPK/ULK1 activation, suggesting that $P2X_7$ positively regulates LL-37–mediated KC autophagy.

Although autophagy is critical for the regulation of the intestinal TJ barrier, the cross-talk between epidermal TJs and autophagy remains unclear. Deficiency of *Atg9A* in intestinal epithelial cells resulted in reduced TER and abnormal distribution of TJ proteins, such as ZO-1 and occludin, indicating that Atg9A is essential for the functional intestinal TJ barrier (Dowdell et al., 2020). Furthermore, autophagy activation enhances TJ barrier function in intestinal epithelial cells by targeting claudin-2 for lysosomal degradation (Nighot et al., 2015). In contrast, antibiotic treatment disrupted TJ protein morphology and activated autophagy in mice, suggesting that autophagy may contribute to a dysfunctional TJ barrier (Feng et al., 2019). Moreover, after burn injury, the activation of autophagy increased the disruption of TJ proteins, whereas the inhibition of autophagy ameliorated TJ protein expression (Huang et al., 2019). Regarding the association between autophagy and epidermal barrier function, it has been shown that Atg7-dependent autophagy was active in differentiating KCs but nonessential for the maintenance of the functional skin barrier (Rossiter et al., 2013). However, whether autophagy influences the epidermal TJ barrier remains unknown. We showed that the LL-37–mediated enhancement in TJ barrier function was abolished in autophagy-deficient KCs and KCs and skin equivalents treated with autophagy inhibitors, indicating that autophagy activation is essential for the LL-37–induced improvement in TJ barrier. *Claudin-1*–deficient mice display severely wrinkled skin and dehydration and die within 1 day of birth (Furuse et al., 2002), and *ZO-1* deficiency leads to an enhanced large solute flux across TJs and delays TJ barrier establishment (Umeda et al., 2004; Van Itallie et al., 2009). The finding that LL-37–mediated autophagy regulates the distribution of TJ-related proteins and TJ barrier function suggests that autophagy is involved in epidermal TJ barrier maintenance. Surprisingly, LL-37 had no effect on desmosomal and adherens junction proteins. The effect of LL-37 on desmosomal and adherens junctions needs to be investigated further.

Previous studies showed that LL-37 contributes to improvement in the epidermal barrier and differentiation (Aberg et al., 2008; Akiyama et al., 2014). Because LL-37 activates KC autophagy, LL-37 may be a potential target for the treatment of skin diseases, such as psoriasis and AD, which are characterized by a compromised epidermal barrier and autophagy; however, further investigations are needed to confirm this hypothesis.

MATERIALS AND METHODS

Materials and reagents

The details of the reagents and antibodies are described in the Supplementary Materials and Methods. Written informed consent was not necessary because human KCs and skin equivalents used in this study were purchased from suppliers.

KC culture and stimulation

Primary human epidermal KCs (Kurabo Industries, Osaka, Japan) were cultured in serum-free KC growth medium, HuMedia-KG2 (Kurabo Industries). The Ca^{2+} concentration in HuMedia-KG2 was 0.15 mM. For the TJ protein expression and TER assays, KCs were switched to high extracellular Ca^{2+} (1.8 mM) concentration medium.

Western blot analysis

Cells were lysed and proteins were subjected to SDS-PAGE. The blots were incubated with primary antibodies and imaged as described in Supplementary Materials and Methods.

Immunofluorescence staining

KCs cultured on micro cover glasses and paraffin sections of skin equivalents were fixed, blocked, and visualized with antibodies. For details, see Supplementary Materials and Methods.

Electron microscopy

Cells cultured on micro cover glasses were fixed and imaged under an electron microscope. For details, see Supplementary Materials and Methods.

Adenovirus-mediated silencing of gene expression

To express exogenous Atg3C264S proteins, KCs were plated on six-well dishes in 2 ml of growth medium for 24 hours before infection. The medium was replaced with fresh medium containing Atg3C264S adenovirus. After 24 hours, the cells were lysed or treated with LL-37 for the western blot or immunofluorescence analysis.

Measurements of TER

KCs grown on 0.65-cm^2 Transwell filters were transferred into a medium containing high Ca^{2+}, and stimulants were added to both the apical and basal compartments. The TER was measured using a cellZscope (NanoAnalytics, Münster, Germany) for 96 hours after the stimulation as previously reported (Akiyama et al., 2014).

Human skin equivalent models

LabCyte EPI-Model24 (J-Tec, Aichi, Japan), consisting of normal human epidermal KCs cultured to form a multilayer, has been shown to provide a highly differentiated model of the human epidermis after 1 week of culture (Kojima et al., 2012). These three-dimensional skin equivalent models were created from scratch and were not fully developed upon arrival. The air-lifted tissues (day 0) were aseptically removed from the agarose transport medium, transferred into 24-well plates with assay medium, and incubated until stimulation. On day 2 or day 4, the tissues were exposed to various reagents for 72-hour treatment and fixed with 4% paraformaldehyde in PBS. The tissue sections were used for H&E, immunohistochemistry, and immunofluorescence stainings.

TJ permeability assay

The TJ permeability assay was performed using EZ-link Sulfo-NHS-LC-Biotin (Thermo Fisher Scientific, Waltham, MA) as a paracellular tracer in skin equivalents as previously described (Yuki et al., 2011). For details, see Supplementary Materials and Methods.

H&E staining and immunohistochemistry staining

Paraffin sections of skin equivalents were stained with H&E or immunohistochemistry staining as described in the Supplementary Materials and Methods.

Statistical analysis

The statistical analysis was performed using ANOVA, followed by the appropriate posthoc test or Student's *t*-test with GraphPad Prism (Prism 9, GraphPad Software, San Diego, CA). $P < 0.05$ were considered significant. The results are shown as the means ± SD.

Data availability statement

No datasets were generated or analyzed during this study.

ORCIDs
Risa Ikutama: http://orcid.org/0000-0002-4407-6969
Ge Peng: http://orcid.org/0000-0002-3278-2604
Saya Tsukamoto: http://orcid.org/0000-0003-3947-3369
Yoshie Umehara: http://orcid.org/0000-0001-9039-0644
Juan V. Trujillo-Paez: http://orcid.org/0000-0002-4749-1201
Hainan Yue: http://orcid.org/0000-0001-8982-3334
Hai Le Thanh Nguyen: http://orcid.org/0000-0002-9566-2458
Miho Takahashi: http://orcid.org/0000-0002-4483-3894
Shun Kageyama: http://orcid.org/0000-0001-5673-9734
Masaaki Komatsu: http://orcid.org/0000-0001-7672-7722
Ko Okumura: http://orcid.org/0000-0003-3238-6422
Hideoki Ogawa: http://orcid.org/0000-0003-4268-8790
Shigaku Ikeda: http://orcid.org/0000-0002-7520-0707
François Niyonsaba: http://orcid.org/0000-0002-0588-8315

CONFLICT OF INTEREST
The authors state no conflict of interest.

ACKNOWLEDGMENTS
This work was partially supported by a Grant-in-Aid for Scientific Research from the Ministry of Education, Culture, Sports, Science and Technology of Japan to FN (grant number 26461703 and 21K08309), a grant from the National Eczema Association (grant number NEA21-ERG159) and Vichy Exposome Grant to GP. We thank Michiyo Matsumoto for the secretarial assistance and Eri Yoshimoto for the technical support.

AUTHOR CONTRIBUTIONS
Conceptualization: RI, GP, SK, MK, KO, HO, SI, FN; Data Curation: RI, GP, ST, YU, HLTN, JVTP, SK, HY, MT; Funding Acquisition: GP, KO, HO, SI, FN; Methodology: RI, GP, ST, YU, HLTN, JVTP, SK, HY, MT; Supervision: KO, HO, SI, FN; Visualization: RI, GP, ST, SK, MK; Writing - Original Draft Preparation: RI, GP, SK, MK; Writing - Review and Editing: RI, GP, SK, MK, KO, HO, SI, FN

SUPPLEMENTARY MATERIAL
Supplementary material is linked to the online version of the paper at www.jidonline.org, and at https://doi.org/10.1016/j.jid.2022.10.020.

REFERENCES
Aberg KM, Man MQ, Gallo RL, Ganz T, Crumrine D, Brown BE, et al. Co-regulation and interdependence of the mammalian epidermal permeability and antimicrobial barriers. J Invest Dermatol 2008;128:917–25.

Akinduro O, Sully K, Patel A, Robinson DJ, Chikh A, McPhail G, et al. Constitutive autophagy and nucleophagy during epidermal differentiation. J Invest Dermatol 2016;136:1460–70.

Akiyama T, Niyonsaba F, Kiatsurayanon C, Nguyen TT, Ushio H, Fujimura T, et al. The human cathelicidin LL-37 host defense peptide upregulates tight junction-related proteins and increases human epidermal keratinocyte barrier function. J Innate Immun 2014;6:739–53.

Bian S, Sun X, Bai A, Zhang C, Li L, Enjyoji K, et al. P2X7 integrates PI3K/AKT and AMPK-PRAS40-mTOR signaling pathways to mediate tumor cell death. PLoS One 2013;8:e60184.

Chieosilapatham P, Ikeda S, Ogawa H, Niyonsaba F. Tissue-specific regulation of innate immune responses by human cathelicidin LL-37. Curr Pharm Des 2018;24:1079–91.

Douroudis K, Kingo K, Traks T, Reimann E, Raud K, Rätsep R, et al. Polymorphisms in the ATG16L1 gene are associated with psoriasis vulgaris. Acta Derm Venereol 2012;92:85–7.

Dowdell AS, Cartwright IM, Goldberg MS, Kostelecky R, Ross T, Welch N, et al. The HIF target ATG9A is essential for epithelial barrier function and tight junction biogenesis. Mol Biol Cell 2020;31:2249–58.

Elssner A, Duncan M, Gavrilin M, Wewers MD. A novel P2X7 receptor activator, the human cathelicidin-derived peptide LL37, induces IL-1 beta processing and release. J Immunol 2004;172:4987–94.

Fabbrizio P, Amadio S, Apolloni S, Volonté C. P2X7 receptor activation modulates autophagy in SOD1-G93A mouse microglia. Front Cell Neurosci 2017;11:249.

Fan XY, Tian C, Wang H, Xu Y, Ren K, Zhang BY, et al. Activation of the AMPK-ULK1 pathway plays an important role in autophagy during prion infection. Sci Rep 2015;5:14728.

Feng Y, Huang Y, Wang Y, Wang P, Song H, Wang F. Antibiotics induced intestinal tight junction barrier dysfunction is associated with microbiota dysbiosis, activated NLRP3 inflammasome and autophagy. PLoS One 2019;14:e0218384.

Furuse M, Hata M, Furuse K, Yoshida Y, Haratake A, Sugitani Y, et al. Claudin-based tight junctions are crucial for the mammalian epidermal barrier: a lesson from claudin-1-deficient mice. J Cell Biol 2002;156:1099–111.

Hara T, Nakamura K, Matsui M, Yamamoto A, Nakahara Y, Suzuki-Migishima R, et al. Suppression of basal autophagy in neural cells causes neurodegenerative disease in mice. Nature 2006;441:885–9.

Harris J. Autophagy and cytokines. Cytokine 2011;56:140–4.

Huang Y, Wang Y, Feng Y, Wang P, He X, Ren H, et al. Role of endoplasmic reticulum stress-autophagy axis in severe burn-induced intestinal tight junction barrier dysfunction in mice. Front Physiol 2019;10:606.

Kabeya Y, Mizushima N, Ueno T, Yamamoto A, Kirisako T, Noda T, et al. LC3, a mammalian homologue of yeast Apg8p, is localized in autophagosome membranes after processing [published correction appears in EMBO J 2003;22:4577] EMBO J 2000;(19):5720–8.

Kim GK, Del Rosso JQ. Drug-provoked psoriasis: is it drug induced or drug aggravated?: understanding pathophysiology and clinical relevance. J Clin Aesthet Dermatol 2010;3:32–8.

Kim HR, Kim JC, Kang SY, Kim HO, Park CW, Chung BY. Rapamycin alleviates 2,3,7,8-tetrachlorodibenzo-p-dioxin-induced aggravated dermatitis in mice with imiquimod-induced psoriasis-like fermatitis by inducing sutophagy. Int J Mol Sci 2021;22:3968.

Kim J, Kundu M, Viollet B, Guan KL. AMPK and mTOR regulate autophagy through direct phosphorylation of Ulk1. Nat Cell Biol 2011;13:132–41.

Klapan K, Frangež Ž, Markov N, Yousefi S, Simon D, Simon HU. Evidence for lysosomal dysfunction within the epidermis in psoriasis and atopic dermatitis. J Invest Dermatol 2021;141:2838–48.e4.

Klionsky DJ, Abdel-Aziz AK, Abdelfatah S, Abdellatif M, Abdoli A, Abel S, et al. Guidelines for the use and interpretation of assays for monitoring autophagy (4th edition)[1]. Autophagy 2021;17:1–382.

Klionsky DJ, Emr SD. Autophagy as a regulated pathway of cellular degradation. Science 2000;290:1717–21.

Kojima H, Ando Y, Idehara K, Katoh M, Kosaka T, Miyaoka E, et al. Validation study of the in vitro skin irritation test with the LabCyte EPI-MODEL24. Altern Lab Anim 2012;40:33–50.

Koria P, Andreadis ST. Epidermal morphogenesis: the transcriptional program of human keratinocytes during stratification. J Invest Dermatol 2006;126:1834–41.

Kuroda K, Okumura K, Isogai H, Isogai E. The human cathelicidin antimicrobial peptide LL-37 and mimics are potential anticancer drugs. Front Oncol 2015;5:144.

Lee HM, Shin DM, Yuk JM, Shi G, Choi DK, Lee SH, et al. Autophagy negatively regulates keratinocyte inflammatory responses via scaffolding protein p62/SQSTM1. J Immunol 2011;186:1248–58.

Lee Y, Shin K, Shin KO, Yoon S, Jung J, Hwang E, et al. Topical application of autophagy-activating peptide improved skin barrier function and reduced acne symptoms in acne-prone skin. J Cosmet Dermatol 2021;20:1009–16.

Li C, Johnson DE. Bortezomib induces autophagy in head and neck squamous cell carcinoma cells via JNK activation. Cancer Lett 2012;314:102–7.

Murakami M, Ohtake T, Dorschner RA, Schittek B, Garbe C, Gallo RL. Cathelicidin anti-microbial peptide expression in sweat, an innate defense system for the skin. J Invest Dermatol 2002;119:1090–5.

Nighot PK, Hu CA, Ma TY. Autophagy enhances intestinal epithelial tight junction barrier function by targeting claudin-2 protein degradation. J Biol Chem 2015;290:7234–46.

Niyonsaba F, Kiatsurayanon C, Chieosilapatham P, Ogawa H. Friends or foes? Host defense (antimicrobial) peptides and proteins in human skin diseases. Exp Dermatol 2017;26:989–98.

Ohsumi Y. Molecular dissection of autophagy: two ubiquitin-like systems. Nat Rev Mol Cell Biol 2001;2:211–6.

Ong PY, Ohtake T, Brandt C, Strickland I, Boguniewicz M, Ganz T, et al. Endogenous antimicrobial peptides and skin infections in atopic dermatitis. N Engl J Med 2002;347:1151–60.

Peng G, Tsukamoto S, Ikutama R, Nguyen HLT, Umehara Y, Trujillo-Paez JV, et al. Human β-defensin-3 attenuates atopic dermatitis-like inflammation through autophagy activation and the aryl hydrocarbon receptor signaling pathway. J Clin Invest 2022;132:e156501.

Rekha RS, Rao Muvva SS, Wan M, Raqib R, Bergman P, Brighenti S, et al. Phenylbutyrate induces LL-37-dependent autophagy and intracellular killing of Mycobacterium tuberculosis in human macrophages. Autophagy 2015;11:1688–99.

Rogov V, Dötsch V, Johansen T, Kirkin V. Interactions between autophagy receptors and ubiquitin-like proteins form the molecular basis for selective autophagy. Mol Cell 2014;53:167–78.

Rossiter H, König U, Barresi C, Buchberger M, Ghannadan M, Zhang CF, et al. Epidermal keratinocytes form a functional skin barrier in the absence of Atg7 dependent autophagy. J Dermatol Sci 2013;71:67–75.

Schmeisser K, Parker JA. Pleiotropic effects of mTOR and autophagy during development and aging. Front Cell Dev Biol 2019;7:192.

Sou YS, Waguri S, Iwata J, Ueno T, Fujimura T, Hara T, et al. The Atg8 conjugation system is indispensable for proper development of autophagic isolation membranes in mice. Mol Biol Cell 2008;19:4762–75.

Sukseree S, Bakiri L, Palomo-Irigoyen M, Uluçkan Ö, Petzelbauer P, Wagner EF. Sequestosome 1/p62 enhances chronic skin inflammation. J Allergy Clin Immunol 2021;147:2386–93.e4.

Sun T, Li D, Wang L, Xia L, Ma J, Guan Z, et al. C-Jun NH2-terminal kinase activation is essential for up-regulation of LC3 during ceramide-induced autophagy in human nasopharyngeal carcinoma cells. J Transl Med 2011;9:161.

Tong Y, Huang H, Pan H. Inhibition of MEK/ERK activation attenuates autophagy and potentiates pemetrexed-induced activity against HepG2 hepatocellular carcinoma cells. Biochem Biophys Res Commun 2015;456:86–91.

Umeda K, Matsui T, Nakayama M, Furuse K, Sasaki H, Furuse M, et al. Establishment and characterization of cultured epithelial cells lacking expression of ZO-1. J Biol Chem 2004;279:44785–94.

Van Itallie CM, Fanning AS, Bridges A, Anderson JM. ZO-1 stabilizes the tight junction solute barrier through coupling to the perijunctional cytoskeleton. Mol Biol Cell 2009;20:3930–40.

Wang Y, Zhang H. Regulation of autophagy by mTOR signaling pathway. Adv Exp Med Biol 2019;1206:67–83.

Wang Z, Zhou H, Zheng H, Zhou X, Shen G, Teng X, et al. Autophagy-based unconventional secretion of HMGB1 by keratinocytes plays a pivotal role in psoriatic skin inflammation. Autophagy 2021;17:529–52.

Ye YC, Yu L, Wang HJ, Tashiro S, Onodera S, Ikejima T. TNFα-induced necroptosis and autophagy via supression of the p38-NF-κB survival pathway in L929 cells. J Pharmacol Sci 2011;117:160–9.

Yoshida K, Yokouchi M, Nagao K, Ishii K, Amagai M, Kubo A. Functional tight junction barrier localizes in the second layer of the stratum granulosum of human epidermis. J Dermatol Sci 2013;71:89–99.

Yoshii SR, Mizushima N. Monitoring and measuring autophagy. Int J Mol Sci 2017;18:1865.

Young CN, Sinadinos A, Lefebvre A, Chan P, Arkle S, Vaudry D, et al. A novel mechanism of autophagic cell death in dystrophic muscle regulated by P2RX7 receptor large-pore formation and HSP90. Autophagy 2015;11:113–30.

Yuk JM, Shin DM, Lee HM, Yang CS, Jin HS, Kim KK, et al. Vitamin D3 induces autophagy in human monocytes/macrophages via cathelicidin. Cell Host Microbe 2009;6:231–43.

Yuki T, Hachiya A, Kusaka A, Sriwiriyanont P, Visscher MO, Morita K, et al. Characterization of tight junctions and their disruption by UVB in human epidermis and cultured keratinocytes. J Invest Dermatol 2011;131:744–52.

Yuki T, Haratake A, Koishikawa H, Morita K, Miyachi Y, Inoue S. Tight junction proteins in keratinocytes: localization and contribution to barrier function. Exp Dermatol 2007;16:324–30.

Zhao L, Cui L, Jiang X, Zhang J, Zhu M, Jia J, et al. Extracellular pH regulates autophagy via the AMPK-ULK1 pathway in rat cardiomyocytes. FEBS Lett 2016;590:3202–12.

Zhou C, Zhou J, Sheng F, Zhu H, Deng X, Xia B, et al. The heme oxygenase-1 inhibitor ZnPPIX induces non-canonical, Beclin 1-independent, autophagy through p38 MAPK pathway. Acta Biochim Biophys Sin (Shanghai) 2012;44:815–22.

SUPPLEMENTARY MATERIALS AND METHODS

Reagents

The antimicrobial peptide LL-37 (L^{1}LGDFFRKSKEKIGKEFKRIVQRIKDFLRNLVPRTES^{37}) was synthesized by the solid-phase method as previously reported (Akiyama et al., 2014). Anti-LC3 antibody was purchased from MBL International (Woburn, MA). Sequestosome 1/p62, phosphorylated mTOR, phosphorylated p70 S6 kinase (Thr389), phosphorylated p70 S6 kinase (Thr421/Ser424), p70 S6 kinase, phosphorylated adenosine monophosphate–activated protein kinase, phosphorylated unc-51-like kinase 1 (Ser757), phosphorylated SAPK/c-Jun NH_2-terminal kinase, SAPK/c-Jun NH_2-terminal kinase, phosphorylated p38, p38, phosphorylated extracellular signal–regulated kinase 1/2, extracellular signal–regulated kinase, phosphorylated β-catenin, and β-catenin antibodies were obtained from Cell Signaling Technology (Beverly, MA). Adenosine monophosphate–activated protein kinase 1/2, LAMP-1, unc-51-like kinase 1, involucrin, desmoglein 1, desmocollin 1, and desmocollin 1 antibodies were purchased from Santa Cruz Biotechnology (Dallas, TX). Antibodies against claudin-1, claudin-4, ZO-1, occludin, Ki-67, and E-cadherin were purchased from Invitrogen (Carlsbad, CA). Keratin 1 and keratin 5 antibodies were purchased from BioLegend (San Diego, CA). Keratin 10 antibody was purchased from Novus Biologicals (Littleton, CO), whereas keratin 14 antibody was obtained from PROGEN (Heidelberg, Germany). Phosphorylated E-cadherin and FLG antibodies were purchased from Abcam (Cambridge, United Kingdom), whereas transglutaminase 1 antibody was from Proteintech (Rosemont, IL). E64d and pepstatin A were obtained from the Peptide Institute (Osaka, Japan). KN-62 was obtained from Cayman Chemical (Ann Arbor, MS); Compound C was purchased from Tokyo Chemical Industry (Tokyo, Japan); SBI-0206965 was obtained from Selleckchem (Houston, TX); and U0126, SB203580, and c-Jun NH_2-terminal kinase inhibitor II were purchased from Calbiochem-Novabiochem (La Jolla, CA). Chloroquine and wortmannin were purchased from Sigma—Aldrich (St. Louis, MO). An adenovirus expression vector kit from Takara Bio (Shiga, Japan) was used to prepare Atg3C264S adenovirus. The dilution factor of each reagent is shown in Supplementary Table S1.

Western blot analysis

Cells were lysed in RIPA buffer (Cell Signaling Technology, Danvers, MA), and the total protein concentrations were calibrated to be identical and subjected to SDS-PAGE, followed by transfer to methanol-preactivated polyvinylidene difluoride membranes (MilliporeSigma, Billerica, MA). The blots were incubated with primary antibodies overnight at 4 °C according to the manufacturer's instructions. The membranes were developed using Luminata Forte Western HRP substrate (MilliporeSigma) and imaged using the software program Image Gauge, LAS-4000plus (Fujifilm, Tokyo, Japan). The densitometry of the intensity of the bands was analyzed with ImageJ software (National Institutes of Health, Bethesda, MD).

Immunofluorescence microscopy

Keratinocytes were cultured on 12 mm micro cover glasses before fixation with 4% paraformaldehyde in PBS (Fujifilm, Tokyo, Japan). The cells were blocked in Immuno-Block and then incubated overnight at 4 °C with the appropriate primary antibodies in Can Get Signal Solution 1 (Toyobo, Osaka, Japan), followed by secondary antibodies coupled to Alexa 488 and/or Alexa 594 from Invitrogen. Images were captured using confocal laser scanning microscopy (Carl Zeiss, Jena, Germany).

Electron microscopy

Cells cultured on 12 mm micro cover glasses were fixed with 2.5% glutaraldehyde buffered in 0.1 M phosphate buffer at 4 °C overnight. Images were obtained under an HT7700 electron microscope (Hitachi, Tokyo, Japan). Digital images were analyzed using a point-counting method (Ylä-Anttila et al., 2009). Micrographs were assessed by two independent investigators.

Tight Junction permeability assay

The tight junction permeability assay was performed using EZ-link Sulfo-NHS-LC-Biotin (Thermo Fisher Scientific, Waltham, MA) as a paracellular tracer in skin equivalents as previously described (Yuki et al., 2011). Briefly, skin equivalents were incubated with 2 mg/ml NHS-LC-Biotin in PBS containing 1 mM calcium chloride from the dermal side for 30 minutes. After incubation, the skin models were placed in a gelatin capsule and snap frozen for cryofixation. The frozen sections were subsequently fixed in 4% paraformaldehyde in PBS for 10 minutes, and immunofluorescence staining was performed. The stops of claudin-1 colocalization with the biotin tracer were quantified.

H&E staining and immunohistochemistry staining

Paraffin sections of skin equivalents (6 μm) were stained with H&E for morphological analysis. For immunohistochemistry analysis, paraffin sections were washed in xylene and hydration in a series of decreasing alcohol dilution and water for deparaffinization. Antigen recovery was performed in citrate buffer, pH 6.0, for 40 minutes at 95 °C. The sections were blocked using Avidin-Biontin Blocking Kit (Vector Laboratories, Burlingame, CA), followed by 2% BSA/PBS for 30 minutes at room temperature, and then incubated overnight at 4 °C with the appropriate primary antibodies. On the next day, sections were inactivated of endogenous peroxidase with 0.3% hydrogen peroxide/methanol, followed by incubation with secondary antibodies and horseradish peroxidase–conjugated streptavidin. The sections were then colored with 3,3′diaminobenzidine solution and counterstained with hematoxylin. Images were acquired by optical microscopy.

SUPPLEMENTARY REFERENCES

Akiyama T, Niyonsaba F, Kiatsurayanon C, Nguyen TT, Ushio H, Fujimura T, et al. The human cathelicidin LL-37 host defense peptide upregulates tight junction-related proteins and increases human epidermal keratinocyte barrier function. J Innate Immun 2014;6:739—53.

Ylä-Anttila P, Vihinen H, Jokitalo E, Eskelinen EL. Monitoring autophagy by electron microscopy in Mammalian cells. Methods Enzymol 2009;452:143—64.

Yuki T, Hachiya A, Kusaka A, Sriwiriyanont P, Visscher MO, Morita K, et al. Characterization of tight junctions and their disruption by UVB in human epidermis and cultured keratinocytes. J Invest Dermatol 2011;131:744—52.

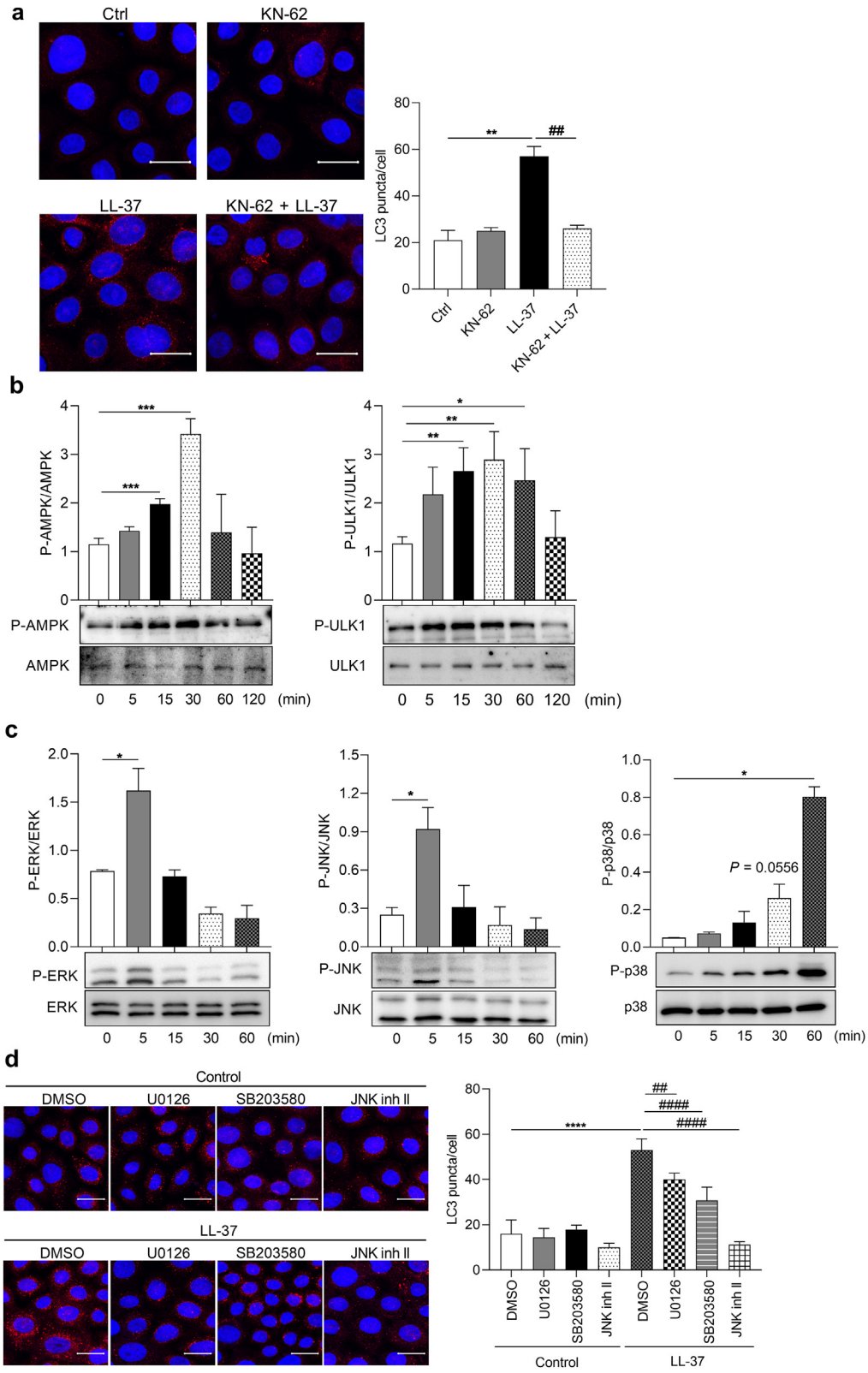

Supplementary Figure S1. Possible pathways of LL-37–induced autophagy in keratinocytes. (**a**) Keratinocytes pretreated with 50 nM KN-62 for 1 hour were incubated with 10 μg/ml LL-37 for 12 hours. LC3 puncta were visualized by immunofluorescence and quantified. (**b**) Keratinocytes were stimulated with 10 μg/ml LL-37, and phosphorylated AMPK and ULK1 were assessed by immunoblotting. (**c**) Keratinocytes were stimulated with 10 μg/ml LL-37 for 5–60 minutes. Phosphorylated ERK, JNK, and p38 were determined by western blotting. The data represent the ratio of phosphorylated ERK, JNK, and unphosphorylated p38 to ERK, JNK, and p38. (**d**) Keratinocytes were pretreated with U0126, SB203580, JNK inh II (2 μM each), or 0.01% DMSO for 2 hours, followed by incubation with 10 μg/ml LL-37 for 12 hours. LC3 puncta were visualized by immunofluorescence staining. $^{*}P < 0.05$, $^{**}P < 0.01$, $^{***}P < 0.001$, $^{****}P < 0.0001$, $^{\#\#}P < 0.01$, and $^{\#\#\#\#}P < 0.0001$. n = 3–4. AMPK, adenosine monophosphate–activated protein kinase; Ctrl, control; ERK, extracellular signal–regulated kinase; JNK, c-Jun NH_2-terminal kinase; JNK inh II, c-Jun NH_2-terminal kinase inhibitor II; min, minute; P-AMPK, phosphorylated adenosine monophosphate–activated protein kinase; P-ERK, phosphorylated extracellular signal–regulated kinase; P-JNK, phosphorylated c-Jun NH_2-terminal kinase; P-p38, phosphorylated p38; P-ULK1, phosphorylated unc-51-like kinase 1; ULK1, unc-51-like kinase 1.

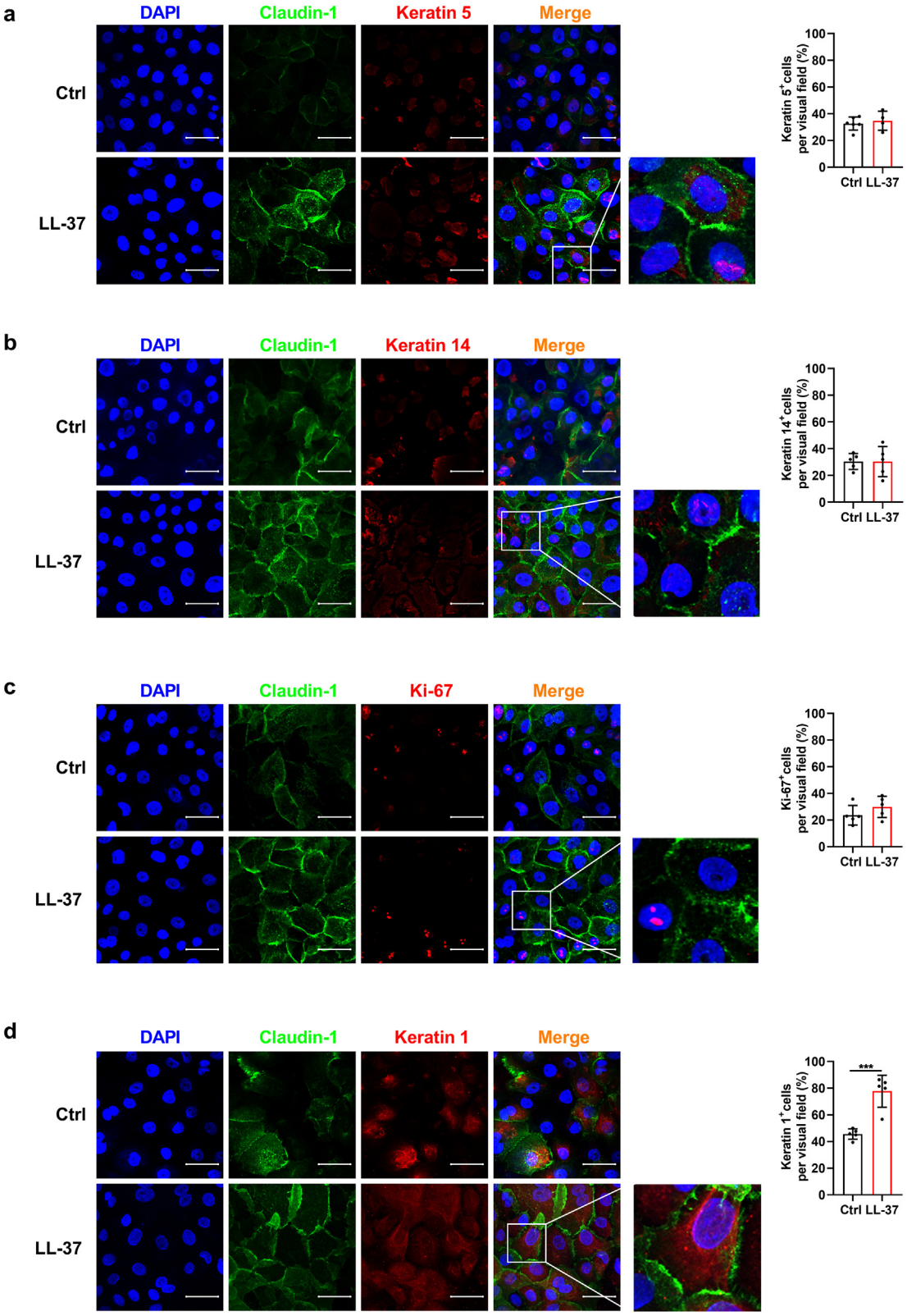

Supplementary Figure S2. Keratinocytes cultured in high extracellular Ca^{2+} concentrations mimic the SG2 cells. Keratinocytes were cultured in high extracellular Ca^{2+} (1.8 mM) concentrations and stimulated with 10 μg/ml LL-37 for 12 hours. The intracellular distribution of claudin-1 and expression of (**a**) keratin 5, (**b**) keratin 14, (**c**) Ki-67, and (**d**) keratin 1 were visualized by immunofluorescence. The right panels show the percentage of keratin 5−, keratin 14−, Ki-67−, and keratin 1−positive cells. ***$P < 0.001$ versus nonstimulated groups. n = 5. Ca^{2+}, calcium ion; Ctrl, control; SG2, second layer of stratum granulosum.

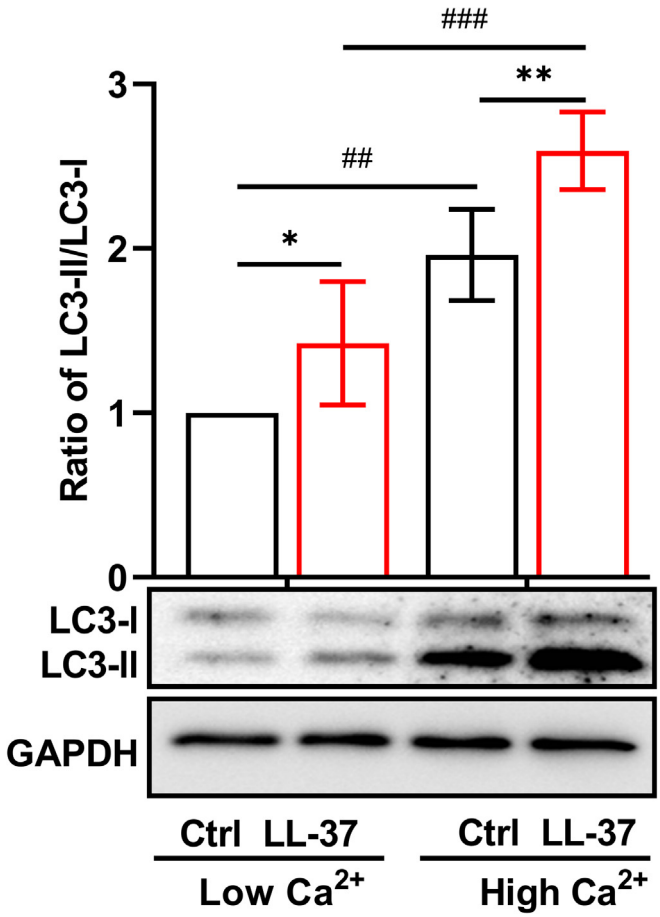

Supplementary Figure S3. LL-37 activates autophagy in differentiated keratinocytes. Keratinocytes were cultured in low Ca^{2+} concentrations (0.15 mM) or high Ca^{2+} concentrations (1.8 mM) and stimulated with 10 μg/ml LL-37 for 12 hours. The expression of LC3-I and LC3-II was determined by immunoblotting. $^{*}P < 0.05$ and $^{**}P < 0.01$ versus the nonstimulated groups and $^{\#\#}P < 0.01$ and $^{\#\#\#}P < 0.001$ versus the groups with low Ca^{2+}. n = 3. Ca^{2+}, calcium ion; Ctrl, control.

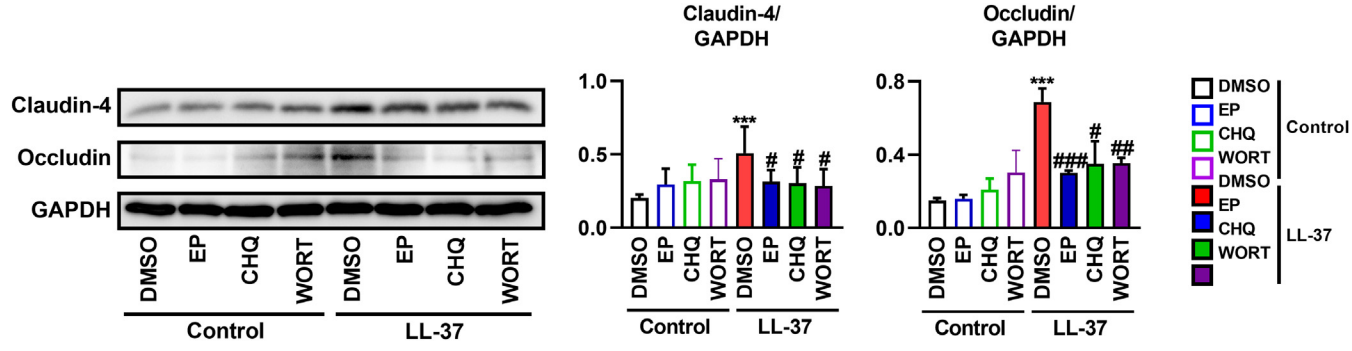

Supplementary Figure S4. LL-37 regulates tight junctions through autophagy activation. Keratinocytes were treated with 10 μg/ml EP, 200 nM CHQ, and 200 nM WORT or 0.1% DMSO for 2 hours and then stimulated with 10 μg/ml LL-37 for 12 hours. Expression of claudin-4 and occludin was determined by immunoblotting. The densitometry of the intensity of the bands was analyzed with ImageJ software (right panels). $^{***}P < 0.001$ versus the nonstimulated groups and $^{\#}P < 0.05$, $^{\#\#}P < 0.01$, and $^{\#\#\#}P < 0.001$ versus the groups without inhibitors. n = 3. CHQ, chloroquine; EP, E64d and pepstatin A; WORT, wortmannin.

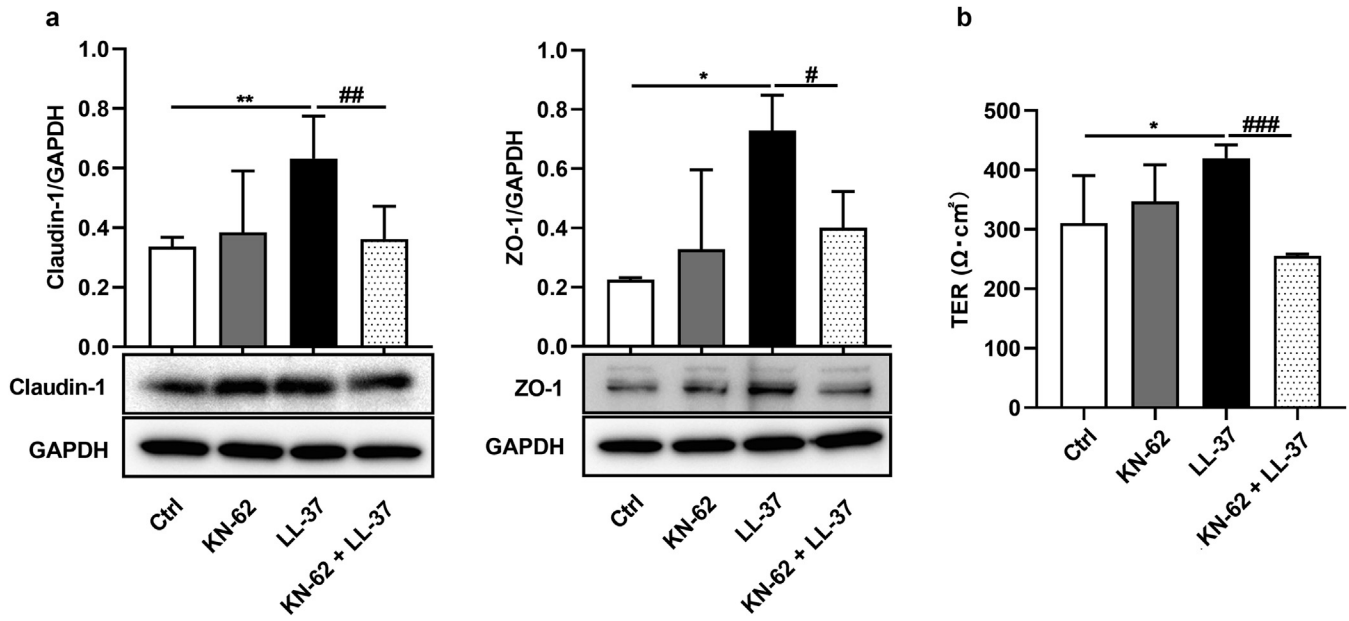

Supplementary Figure S5. LL-37 regulates tight junction proteins through the $P2X_7$ receptor. (**a**) Keratinocytes were pretreated with 50 nM KN-62 for 1 hour, followed by stimulation with 10 μg/ml LL-37 for 12 hours. The expression of claudin-1 and ZO-1 was determined by western blotting. The data represent the ratio of the intensity of claudin-1 and ZO-1 divided by that of GAPDH. (**b**) TER values were also measured in keratinocytes pretreated with KN-62 and stimulated with LL-37. The data represents the TER at 96 hours. $^{*}P < 0.05$ and $^{**}P < 0.01$ versus the nonstimulated groups and $^{\#}P < 0.05$, $^{\#\#}P < 0.01$, and $^{\#\#\#}P < 0.001$ versus the group without KN-62. n = 3. TER, transepithelial electrical resistance.

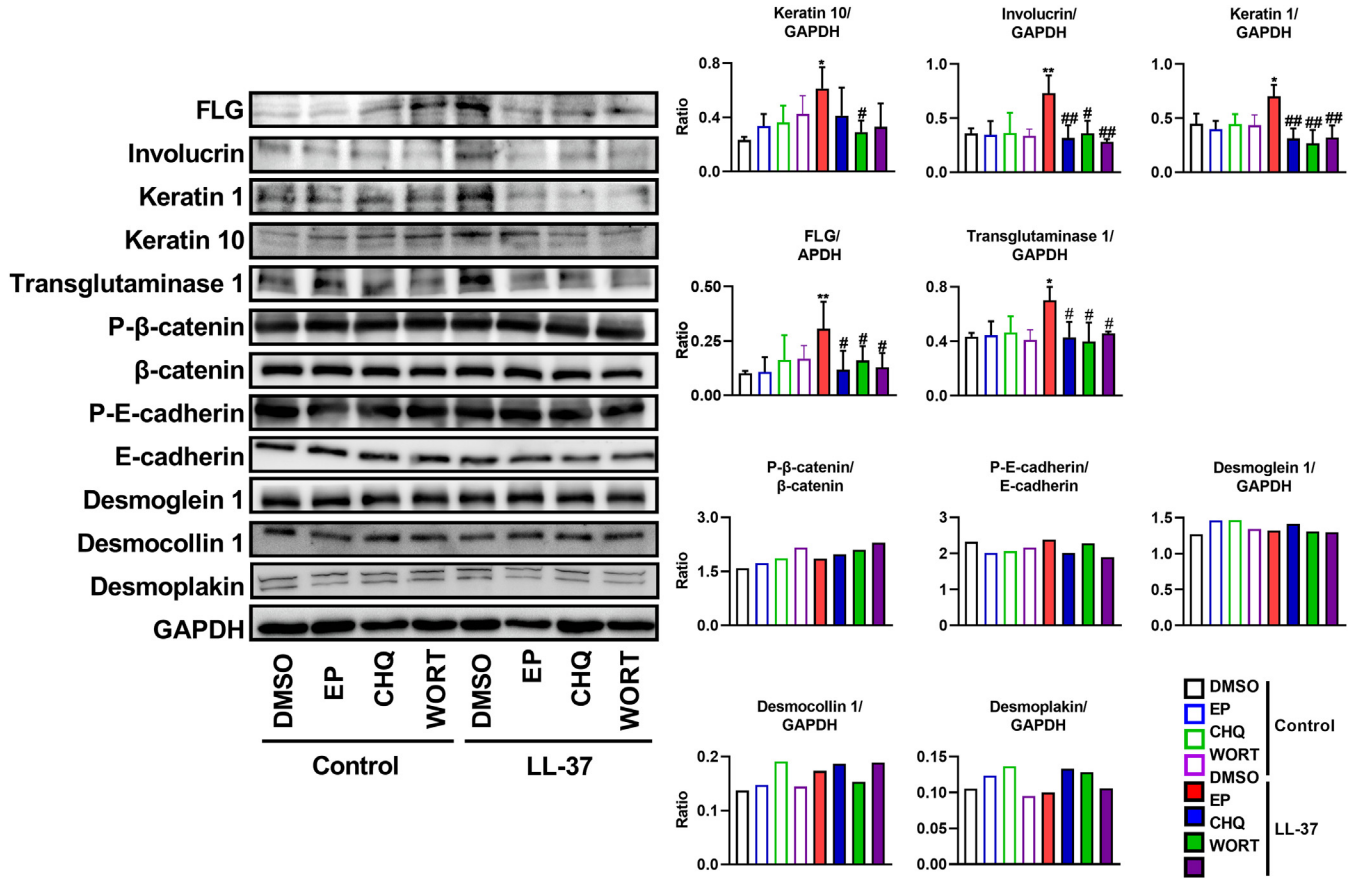

Supplementary Figure S6. Effect of LL-37 on terminal differentiation markers, adherens junction–related proteins, and desmosome-related proteins in keratinocytes. Keratinocytes were treated with 10 mg/ml EP, 200 nM CHQ, and 200 nM WORT or 0.1% DMSO for 2 hours and then stimulated with 10 μg/ml LL-37 for 12 hours. Expression of terminally differentiated markers (FLG, involucrin, keratin 1, keratin 10, and transglutaminase 1), adherens junction–related proteins (β-catenin and E-cadherin), and desmosome-related proteins (desmoglein 1, desmocollin 1, and desmoplakin) was determined by immunoblotting. The densitometry of the intensity of the bands was analyzed with ImageJ software (right panels). $^{*}P < 0.05$ and $^{**}P < 0.01$ versus the nonstimulated groups and $^{\#}P < 0.05$ and $^{\#\#}P < 0.01$ versus the groups without inhibitors. n = 3–5. CHQ, chloroquine; EP, E64d and pepstatin A; P-β-catenin, Phosphorylated β-catenin; P-E-cadherin, phosphorylated E-cadherin; WORT, wortmannin.

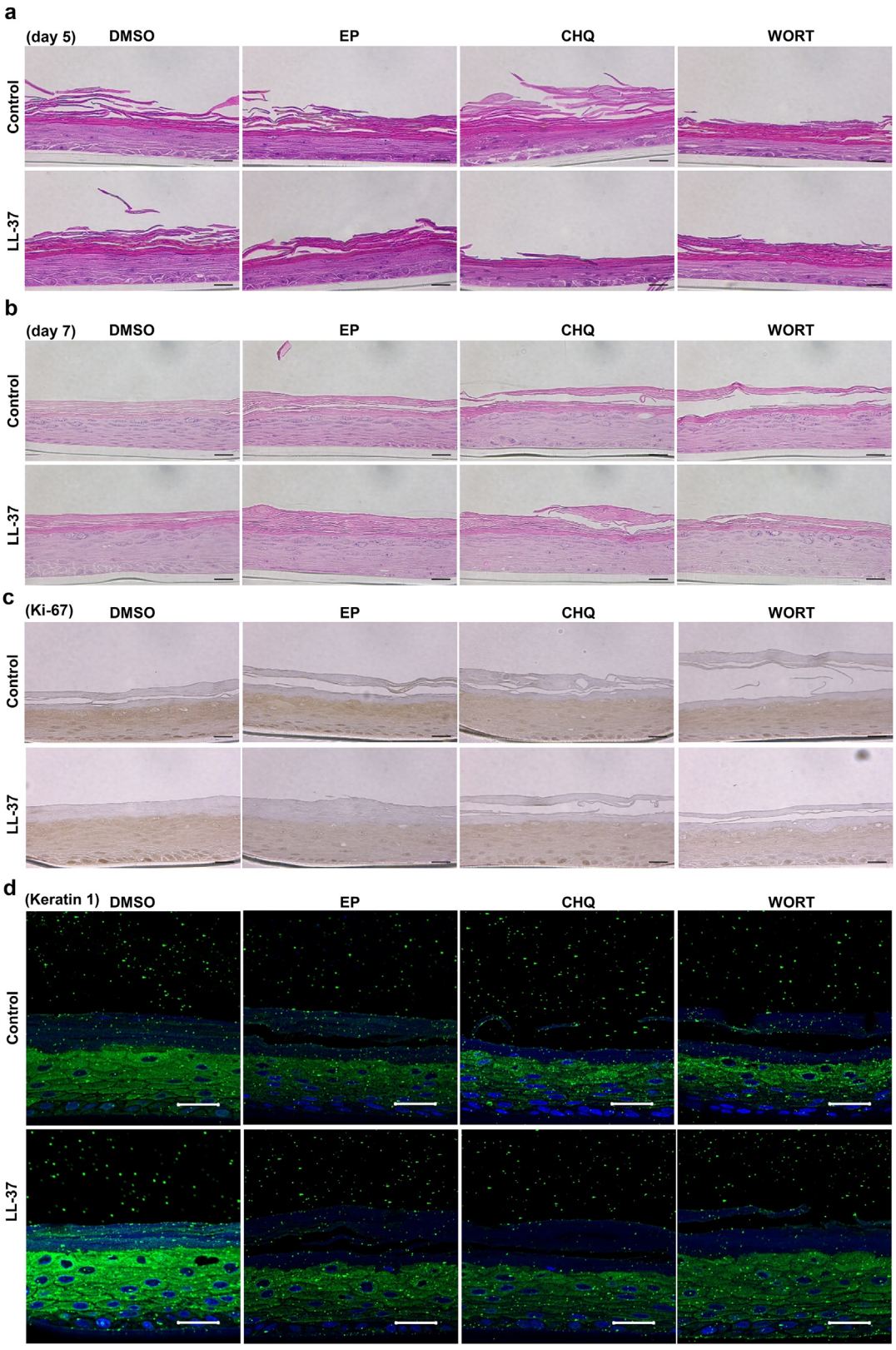

Supplementary Figure S7. H&E staining, proliferation, and differentiation of the skin equivalents. Skin equivalents were treated with 10 μg/ml EP, 200 nM CHQ, and 200 nM WORT or 0.1% DMSO for 2 hours, followed by costimulation with 10 μg/ml LL-37 for 72 hours. Representative H&E staining of the skin models on (**a**) day 5 and (**b**) day 7 is shown. Bar = 200 μm. (**c**) Representative immunohistochemistry images of Ki-67 in skin equivalents. Bar = 200 μm. (**d**) Representative immunofluorescence images of keratin 1 in skin equivalents. Bar = 20 μm. CHQ, chloroquine; EP, E64d and pepstatin A; WORT, wortmannin.